Classical two-center effects in ejected-electron spectra from p^+, p^-, and He^{2+} + He collisions at intermediate energies

C. O. Reinhold and R. E. Olson
Department of Physics, University of Missouri–Rolla, Rolla, Missouri 65401
(Received 5 December 1988)

Doubly and singly differential cross sections for electron emission have been calculated by means of the classical trajectory Monte Carlo method for the p^+, p^-, and He^{2+} + He systems at impact energies of 50 and 100 keV/amu. The calculations for the p^+ and He^{2+} + He systems exhibit the capture to the continuum peak and agree in both shape and magnitude with experimental data. Analysis of the classical trajectories has helped to understand the dynamical formation of this peak. The dependence of the cross sections on the projectile charge (−1, +1, and +2) is analyzed and compared with first-order scalings. It is concluded from this analysis that the combined influence of both the projectile and target Coulomb fields prevails over all the electronic spectra.

I. INTRODUCTION

The study of the combined influence of both the projectile and target Coulomb fields on the electronic spectra has been the central object of recent theoretical as well as experimental works.[1–10] These works have proved that the conventional division of the electronic spectra in electrons captured to the continuum of the projectile or electrons ionized to the continuum of the target is an incomplete description of the ionization process. Comparisons with one-center calculations have demonstrated that two-center effects determine both the shape and magnitude of the electronic spectra at intermediate impact energies.[1,2] Furthermore, the three-body nature of the ionization problem has been revealed by the analysis of the dependence of the cross sections on the projectile charge (Z_p) for ion-atom[2–7] and antimatter-atom[8–10] collisions at intermediate and even high impact energies.

In this work we will present calculations that support the idea that only theories that take into account two-center effects can give a good description of electronic spectra at intermediate impact energies. For this purpose, we shall present doubly and singly differential ionization cross sections (DDCS and SDCS, respectively) as a function of the energy and the angle of the ejected electrons, for collisions of protons (p^+), antiprotons (p^-), and α particles (He^{2+}) with He targets, obtained by means of the classical trajectory Monte Carlo (CTMC) method.[11,12] According to the Z_p^2 scaling predicted by first-order theories, such as the classical binary encounter model or the quantum first Born approximation for direct ionization, there should be no differences between the cross sections for p^+ and p^- projectiles. On the other hand, a factor of 4 is predicted by these theories between the cross sections for the p^+ + He and He^{2+} + He systems. However, as we shall see in Sec. III, large departures from this scaling are observed over all the electronic spectrum.

The CTMC method[11] has proved to be a successful approximation to deal with electron capture and ionization processes in ion-atom collisions at intermediate impact energies. This method has been extensively used to calculate total,[12] singly differential,[2,13] doubly differential,[1,7,14,15] and triply differential[16] cross sections. During the last two years, the CTMC method has also been successfully used to study antimatter-atom collisions.[8,9,17] One of the most important reasons for the success of this approximation is the fact that the electron-incident-ion and electron-target nucleus interactions are exactly taken into account during the collision. This property makes the CTMC method a good candidate to study two-center effects at intermediate energies.

The main purpose of recent papers[1,7,14] concerning CTMC DDCS for ion-atom collisions has been the study of saddle-point electrons, i.e., those electrons with post-collision velocities close to $v_p/2$, v_p being the projectile velocity. As the saddle-point electrons are left stranded between the projectile and the target-core ions, the two-center effects are expected to be very important in this region of the electronic spectra. However, as we shall show in this article, two-center effects are also very important at large ejection angles. Previous articles[8,15,18] presented a disagreement between CTMC SDCS and experimental data of Rudd *et al.*[19–22] at large ejection angles. However, recent experiments[6,23] would indicate that CTMC can account for both SDCS and DDCS at large ejection angles.

The study (by means of the CTMC method) of those electrons that are captured to the continuum of the projectile (i.e., those electrons scattered at small angles with a velocity close to v_p) has been delayed since the statistics of the calculations were insufficient. As it is well known, the DDCS exhibit a sharp peak in this region, which is called the capture to the continuum (CTC) peak.[24] In this article we shall show that this peak is a classical phenomenon and that the CTMC method can predict both its shape and magnitude. This conclusion has been also obtained independently by Montemayor and Schiwietz.[25] The analysis of the classical trajectories has helped us to understand the dynamical formation of this

peak (see Sec. II). The presence of the CTC peak is not a two-center effect since it can be predicted by first-order theories for capture to the continuum of the projectile. However, the asymmetry of the peak (i.e., the Coulombic deformation of the peak due to the residual target core) is a two-center effect. As we shall see, the CTMC method also predicts this asymmetry. Furthermore, this approximation predicts, in agreement with recent experimental data,[6] a very asymmetric dependence of the cross sections on the projectile charge around the CTC peak.

II. THEORY

A three-body CTMC model has been used to obtain the electronic spectra. An effective charge of 1.69 a.u. has been used to represent the He^+ target core. Each electron was supposed to be initially bound to the target core with a binding energy of -0.904 a.u. The cross sections were calculated from the free-electron production channel (i.e., the combination of the single-ionization, double-ionization, and transfer-ionization channels) by means of the independent-electron model (IEM).[18,26] Suppose $P_i(b)$ is the ionization probability as a function of the impact parameter b, N is the total number of trajectories, and $b_{\max}$ is the maximum impact parameter considered (above which ionization is negligible). According to the IEM, the DDCS for free-electron production is given by

$$\frac{d\sigma}{d\Omega dE}=\frac{\sum_k [2-p_i^2(b_k)]}{N\Delta\Omega\Delta E}\pi b_{\max}^2 , \tag{1}$$

where the summation is extended to all the electrons that are detected in the solid angle and energy intervals $(\Omega-\Delta\Omega/2,\Omega+\Delta\Omega/2)$ and $(E-\Delta E/2,E+\Delta E/2)$, which were ionized by projectiles with impact parameters b_k. The ejection angles were determined by means of the final velocities of the electrons.

Present calculations differ from those of Ref. 1 and 7 in that these authors calculated their spectra only from the single-ionization channel. We have included the transfer-ionization and double-ionization channels in our calculations since a better agreement was found between our total electron-emission cross sections for the H^+, $He^{2+}+He$ systems, and the experimental cross sections of Shah and Gilbody.[27] The inclusion of these channels does not appreciably change the DDCS for the H^++He system. However, significant differences were observed for the $He^{2+}+He$ system.

Another difference between previous and present calculations is related to the CTC electrons. We have observed that the dynamical formation of this peak is dominated by two mechanisms. The most important mechanism is a focusing of the electrons in the direction of $\mathbf{v}_p$ due to the interaction with the projectile. We have observed that, in order to decide the final ejection angle of the CTC electrons, it is necessary to integrate the Hamilton equations up to very large internuclear distances. This conclusion agrees with the recent work of Ovchinnikov and Khrebtukov,[28] who predicted that the classical post-collision electron-projectile interaction would produce a pole in the electronic spectra at the position of the CTC peak. A secondary mechanism that contributes to the CTC peak is that a fraction of the electrons that are captured to highly excited states may be ionized by the residual target nucleus still at large internuclear distances. Therefore, it has also been necessary to continue to integrate the equations of motion for those electrons up to very large internuclear distances. This integration has to be carried out with high numerical precision so as not to ionize those electrons due to numerical errors.

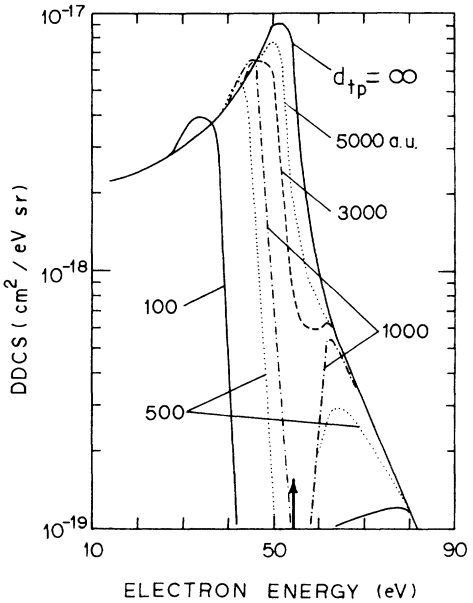

FIG. 1. DDCS for ejection of electrons in collisions of protons with He targets at an impact energy of 100 keV, at an ejection angle of 1°, and as a function of the electron energy. Different curves denote the results that are obtained when the integration of the Hamilton equations is stopped at different final internuclear distances d_{tp}, as indicated. The arrow in the electron energy axis indicates the position where the electron velocity equals the projectile velocity.

In order to illustrate the dynamical formation of the CTC peak, we have plotted in Fig. 1 the energy distribution of the electrons that are detected at 1° for the H^++He system at an impact energy of 100 keV, when the integration of the Hamilton equations is stopped at different internuclear distances of 100, 500, 1000, 3000, 5000, and $+\infty$ a.u. In order to obtain the results for a final infinite internuclear distance, we continued to integrate the equations of the motion analytically. We have checked that the same result is obtained if the numerical integration is continued up to 10^5 a.u. As may be clearly seen in Fig. 1, no CTC peak is obtained if the integration is stopped at internuclear distances less or equal than 1000 a.u. On the contrary, no electrons are detected around the position of the CTC peak. However, as the integration proceeds, electrons previously detected at angles greater than 1° are focused to the direction of $\mathbf{v}_p$.

III. RESULTS AND DISCUSSIONS

We have divided the presentation of our results in three sections. In Sec. III A we demonstrate the ability of

our model to describe the ionization spectra. For this purpose, we compare our absolute DDCS and SDCS with several experimental data for the collisions of protons with He targets. The other two sections are devoted to two-center effects. In Sec. III B we demonstrate the inability of first-order theories to explain the large differences between the electronic spectra for collisions of protons and antiprotons with He targets. This section also contains a discussion about the mechanisms that may be responsible for these differences. The aim of Sec. III C is to analyze the dependence of the cross sections on different positive projectile charges. For this purpose, we compare the ratio between our cross sections for the $He^{2+}+He$ and $p^{+}+He$ systems with very recent experimental data. A brief comment about these ratios has been already presented in a previous paper.[5]

A. Comparison with absolute experimental data for the $p^{+}+He$ system

Figure 2 shows our DDCS for the $p^{+}+He$ system at impact energies of 50 and 100 keV at an ejection angle of 1° and as a function of the electron energy. In order to ensure the statistical error bars shown in the figure, the integration of 10^6 trajectories was required. Our energy and angular acceptances around the CTC peak were set to 2 eV and 2°, respectively. It is clearly seen in this figure that the CTMC approximation predicts the existence of the CTC peak. Moreover, our results are in good agreement in shape and magnitude with recent experimental data of Gibson and Reid[23] and Dahl.[29] Our DDCS at 50 keV present a saddle point at small electron energies. However, it should be noted that this behavior may not exist within our statistical errors.

Figure 2 also shows that our peak and Dahl's peak are slightly more asymmetric than Gibson and Reid's peak. Moreover, a small shift may be observed in the position of the peak. As the ejection angle increases, Fig. 3 shows that a greater shift to lower electron energies appears in the position of the maximum of our DDCS. This behavior is not observed in the data of Gibson and Reid, which predict that the position of the maximum almost does not change for ejection angles smaller than 4°. However, our shifts are consistent with the data of Dahl. This situation may be clearly seen in Fig. 4, where we have plotted the position of the maximum as a function of the ejection angle.

Figures 5 and 6 display our DDCS at impact energies of 50 and 100 keV, respectively, for different ejection angles of 10°, 50°, and 90° and as a function of the electron energy. We compare our results with the experimental data of Gibson and Reid,[23] Rudd *et al.*,[19–22] and Bernardi *et al.*[6] The errors of these data for electron energies greater than 20 eV are less or equal to 20%. On the other hand, the experimental errors at electron energies smaller than 10 eV can be up to 200%. We have not plotted these errors so as to make the figure clear. However, they should be taken into account at the time of making any comparison. The error bars plotted in the figure indicate errors greater than 10% in our curves. In general, there is a good agreement between our results and the experimental data. However, there are large

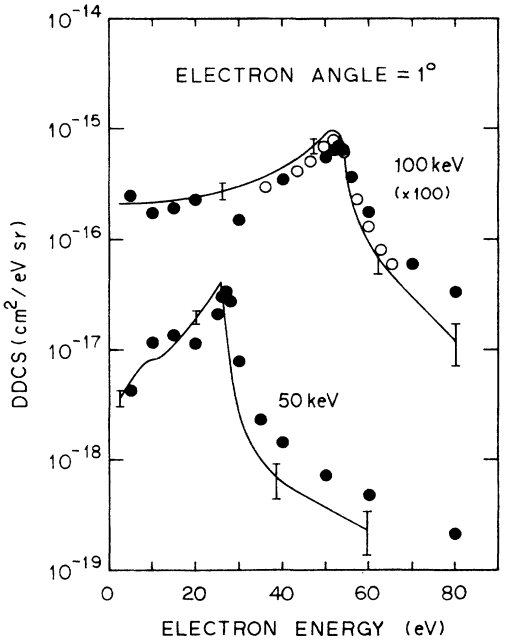

FIG. 2. DDCS for ejection of electrons in collisions of protons with He targets at impact energies of 100 and 50 keV/amu, at an ejection angle of 1°, and as a function of the electron energy. The solid lines denote present CTMC calculations. The angular acceptance of these calculations was 2°. The error bars indicate the statistical errors of our results. Experiments: ●, Gibson and Reid (Ref. 23), ○, Dahl (Ref. 29).

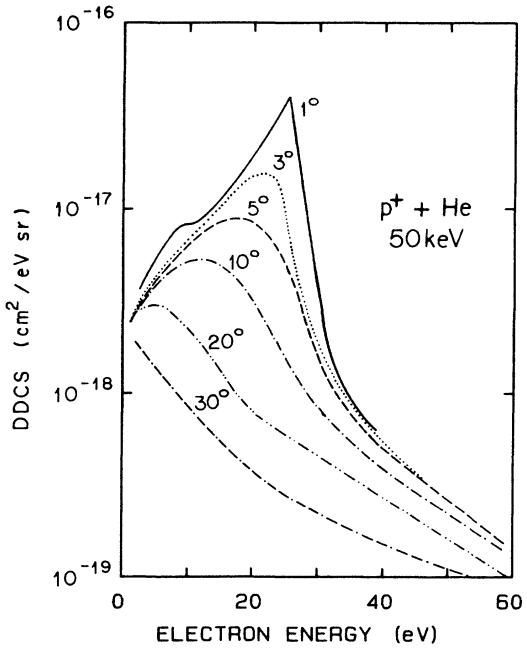

FIG. 3. Present DDCS for ejection of electrons in collisions of protons with He targets at 50 keV/amu for specific angles (as indicated) and as a function of the electron energy.

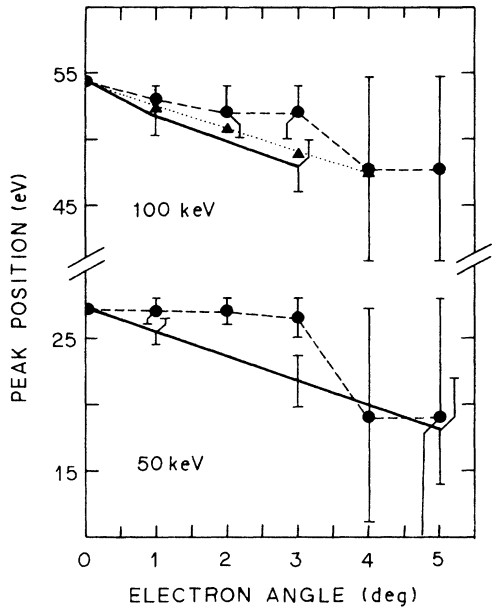

FIG. 4. Position of the maximum of the DDCS as a function of the ejection angle in collisions of protons with He targets at impact energies of 100 and 50 keV, as indicated. The solid lines denote our CTMC calculations. Experiments: · · · ·, ▲, Dahl (Ref. 29); — — —, ●, Gibson and Reid (Ref. 23).

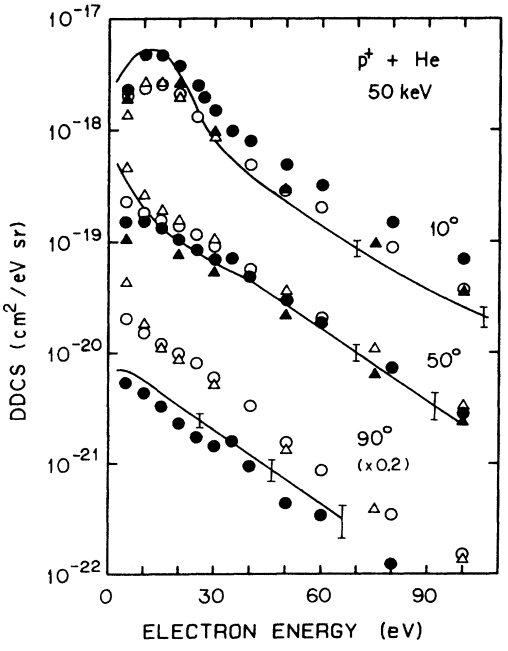

FIG. 5. DDCS for ejection of electrons in collisions of protons with He targets at an impact energy of 50 keV/amu, at ejection angles of 10°, 50°, and 90°, and as a function of the electron energy. The solid lines denote our CTMC calculations. The error bars indicate statistical errors greater than 10% in our results. Experiments: ●, Gibson and Reid (Ref. 23); ▲, Bernardi *et al.* (Ref. 6); △, Rudd and Madison (Ref. 19); ○, Rudd and Jorgensen (Ref. 20).

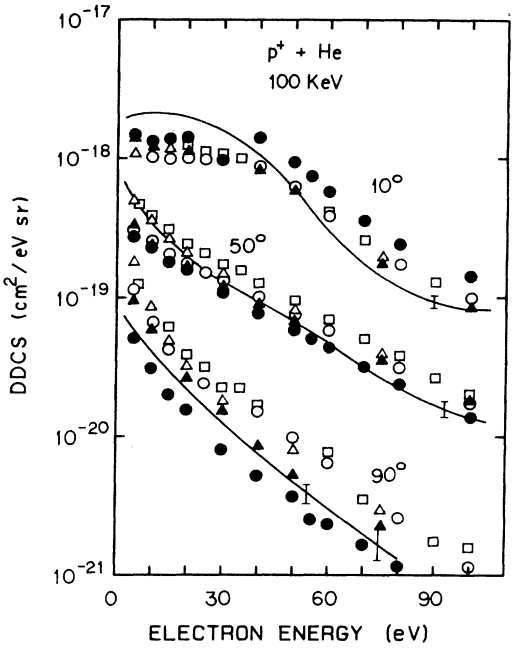

FIG. 6. DDCS for ejection of electrons in collisions of protons with He targets at an impact energy of 100 keV/amu, at ejection angles of 10°, 50°, and 90°, and as a function of the electron energy. The solid lines denote our CTMC calculations. The errors bars indicate statistical errors greater than 10% in our results. Experiments: ●, Gibson and Reid (Ref. 23); ▲, Bernardi *et al.* (Ref. 6); △, Rudd and Madison (Ref. 19); ○, Rudd and Jorgensen (Ref. 20); □, Rudd *et al.* (Ref. 21).

discrepancies between different experimental data. At 10° and small electron energies, our results agree better with Gibson and Reid's data than with Rudd's data. On the other hand, at the same angle and large electron energies, our results agree better with Rudd's and Bernardi's data. A very different situation may be observed at 90°, where our results are in good agreement with Gibson and Reid's and Bernardi's data, which disagree with Rudd's data. This disagreement may be observed more clearly in Fig. 7, in which we compare our SDCS as a function of the ejection angle with the experimental SDCS. In order to obtain Gibson and Reid's SDCS we have integrated their DDCS over the electron energy, using an exponential extrapolation for electron energies smaller than 5 eV or greater than 100 eV. As may be seen in Fig. 7, our results agree with all the experimental data for ejection angles smaller than 60°. However, as the ejection angle is increased, our results and Gibson and Reid's data become very different (up to 400%) from Rudd's data. On the other hand, as may be observed in Fig. 8, these differences are not carried to the SDCS as a function of the electron energy. This figure shows that there is a good agreement between our results and Rudd's data over all the electron energy distributions.

At present it is not possible to decide which of the experimental data are correct at large ejection angles. Our results agree with Gibson and Reid's data. However, we have neglected correlation effects between the two elec-

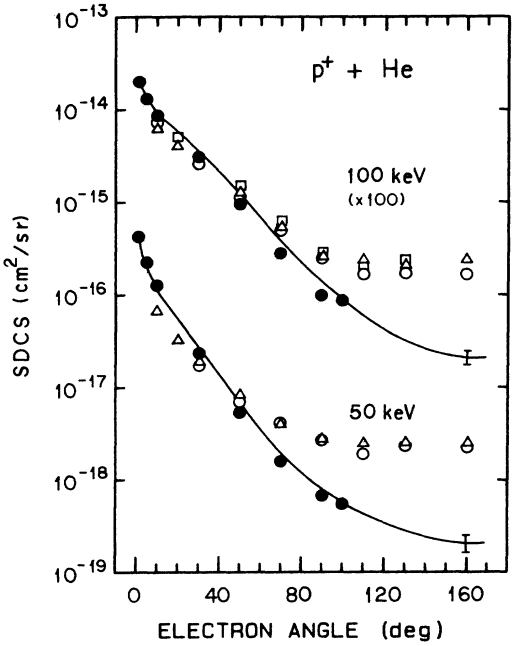

FIG. 7. SDCS for ejection of electrons as a function of the ejection angle in collisions of protons with He targets at impact energies of 50 and 100 keV/amu, as indicated. The solid lines denote our CTMC calculations. The error bars indicate statistical errors greater than 10% in our results. Experiments: ●, Gibson and Reid (Ref. 23); △, Rudd and Madison (Ref. 19); ○, Rudd and Jorgensen (Ref. 20); □, Rudd *et al.* (Ref. 21).

trons of the He atom, i.e., we have used a three-body model and we have represented the nonactive electron by a static effective charge. Rudd and Madison[19] showed that the behavior of the DDCS at large angles is very sensitive to the initial electronic wave function. These authors showed that DDCS obtained with an initial wave function calculated by means of a Hartree-Fock potential are in better agreement with their data at large angles than results obtained by means of an initial single-ζ wave function. However, the theoretical model used by these authors is the first Born approximation for direct ionization, and, as we shall show in the next sections, this model is not appropriate at the impact energies considered. Moreover, Solterfoht *et al.*[3] and Fainstein *et al.*[4] have shown that, also at high impact energies, departures from the first Born approximation are expected at backward angles, as the projectile charge increases.

B. Comparison between the cross sections for the p^+ + He and p^- + He systems

Figure 9 displays our DDCS for the p^+ + He and p^- + He systems at an impact energy of 100 keV/amu for fixed electron energies of 10, 54, and 100 eV. In order to study two-center effects, we have also calculated the cross sections by means of the classical binary encounter (BE) model[30] and the quantum first Born ($B1$) approximation for direct ionization.[19] In order to be sure that the discrepancies between the cross sections are not due to different initial momentum distributions, we have used

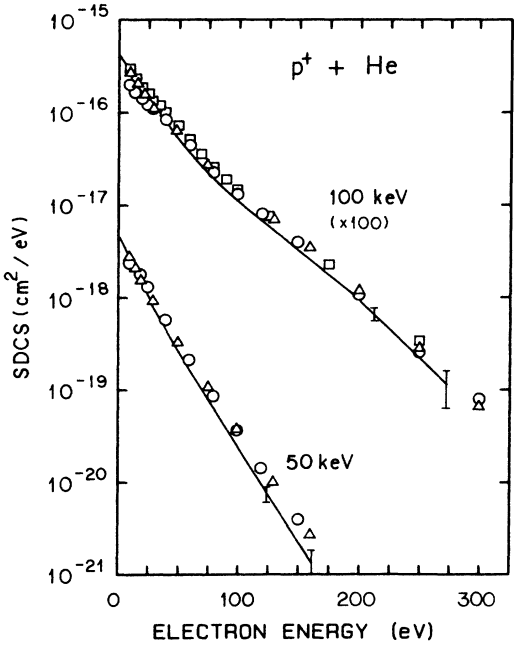

FIG. 8. SDCS for ejection of electrons as a function of the ejection energy in collisions of protons with He targets at impact energies of 50 and 100 keV/amu, as indicated. The solid lines denote our CTMC calculations. The error bars indicate statistical errors greater than 10% in our results. Experiments: △, Rudd and Madison (Ref. 19); ○, Rudd and Jorgensen (Ref. 20); □, Rudd *et al.*, (Ref. 21).

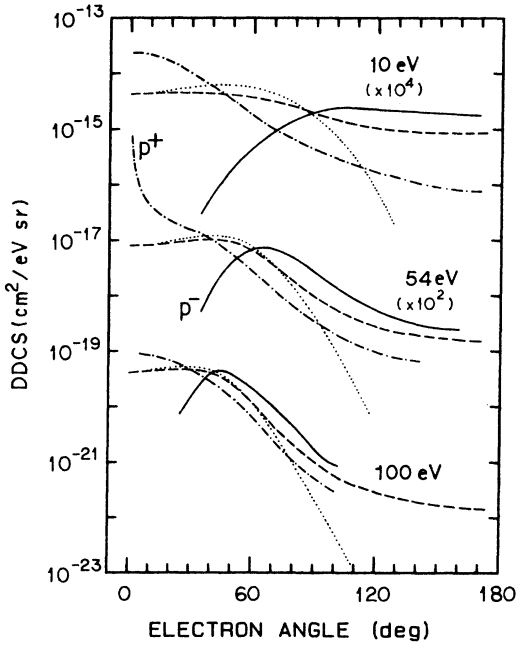

FIG. 9. DDCS for ejection of electrons in collisions of protons and antiprotons with He targets at an impact energy of 100 keV/amu at specific electron energies and as a function of the electron angle. —·—·—·, present CTMC calculations for protons; ——, present CTMC calculations for antiprotons; — — —, present $B1$ calculations for protons and antiprotons; · · · ·, present BE calculations for protons and antiprotons.

the same initial hydrogenic distribution for all the calculations. The difference between $B1$ and BE is the role of the projectile and target nucleus fields in the collision dynamics. While the projectile field is considered to be a perturbation to the initial state in the $B1$ approximation, the BE model considers that this field is the dominant one and neglects the target-nucleus field during the collision dynamics. This is the reason for the falloff of BE DDCS at large ejection angles.

According to $B1$ and BE, the cross sections for p^+ and p^- projectiles should be the same. However, as may be clearly seen in Fig. 9, the CTMC method predicts large departures from this scaling (up to 2 orders in magnitude) over all the electronic spectrum. The regions where these departures are the largest are the forward and the backward ejection angles. These departures may be seen more clearly in Fig. 10, where we have plotted the SDCS as a function of the ejection angle. This figure shows that, while electrons are mostly ejected at small angles for p^+ projectiles, they are primarily ejected at large angles for p^- projectiles. The reason for the differences at small ejection angles may be easily understood: while protons focus electrons in the direction of $\mathbf{v}_p$, antiprotons repel electrons to larger angles. As has been already noticed by previous authors,[10,31] while positive projectiles produce CTC electrons, a dip is obtained at forward angles for negative projectiles.

In general, $B1$ cross sections are between CTMC cross sections for p^+ and p^- projectiles. As the electron energy increases, Fig. 9 seems to indicate that the DDCS for protons and antiprotons would tend to the same values, which would be similar to those obtained with $B1$. The statistics of our calculations were insufficient to obtain DDCS with reasonable error limits at electron energies greater than 100 eV. However, our SDCS as a function of the electron energy (see Fig. 11) shows that differences persist at electron energies higher than 100 eV. Furthermore, this figure shows that, while protons produce more soft electrons than antiprotons, the opposite result is obtained at high electron energies. This conclusion is in agreement with calculations recently performed by Fainstein *et al.*[10] at high impact energies. On the other hand, it should be noted that the energy distribution of the ejected electrons is not as sensitive to the sign of the projectile charge as the angular distribution.

In order to investigate the origin of the differences between the angular and energy distributions for p^+ and p^- projectiles, we have tried to establish a correspondence between the impact parameter and the final angle or energy of the ejected electrons. Figures 12 and 13 show the regions determined by the mean impact parameter plus a standard deviation that lead to a given final electron angle or energy, respectively. Although the standard deviations are very large, some conclusions may be obtained from these figures. Figure 12 shows that a correspondence between impact parameters and electron energies can be established only for the case of p^+ projectiles: while the largest impact parameters are associated with the smallest electron energies, the smallest impact parameters are related to the largest electron energies. Analyses in terms of the impact parameter of the different mechanisms that may lead to ionization have been already made in previous papers.[9,32] At small impact parameters, p^- projectiles are more effective than p^+ projectiles to ionize electrons due to the screening of the target nucleus field produced by antiprotons. On the

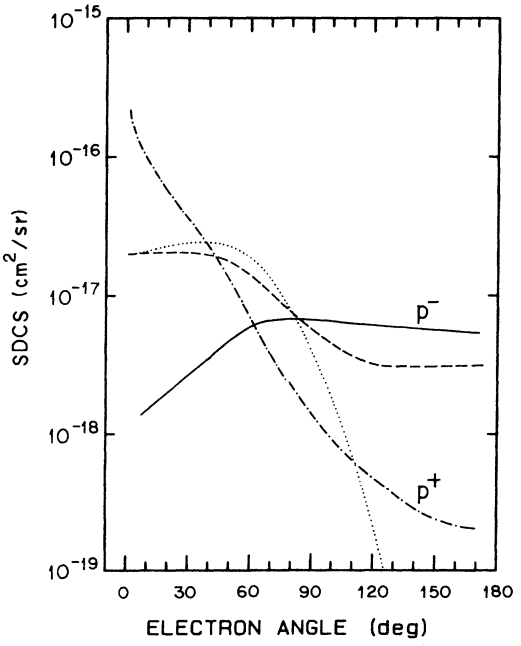

FIG. 10. SDCS for ejection of electrons as a function of the ejection angle in collisions of protons and antiprotons with He targets at an impact energy of 100 keV/amu. The same notation as in Fig. 9 has been used.

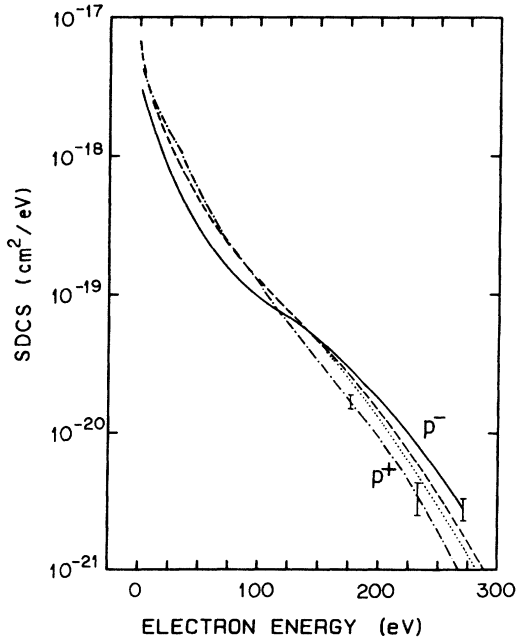

FIG. 11. SDCS for ejection of electrons as a function of the electron energy in collisions of protons and antiprotons with He targets at an impact energy of 100 keV/amu. The same notation as in Fig. 9 has been used.

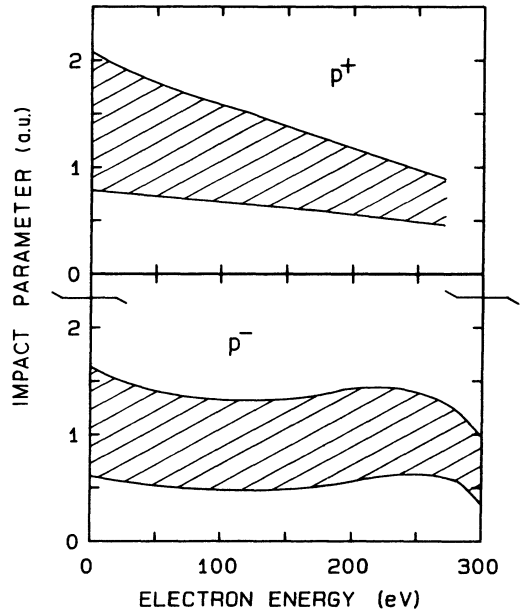

FIG. 12. Regions determined by the mean impact parameter plus a standard deviation that leads to ionized electrons with a certain final energy in collisions of protons and antiprotons with He targets at an impact energy of 100 keV/amu.

other hand, protons are more effective than antiprotons at large impact parameters due to the cancellation of the target nucleus and the projectile Coulombic fields for the electrons that are in between. According to Fig. 12, this may be the mechanism that produces more slow electrons for protons than for antiprotons. Concerning the reason why p^- projectiles produce more fast electrons than p^+ projectiles, Fainstein *et al.*[10] supposed that this behavior was due to the screening effect mentioned above. According to Fig. 12, this would not be the reason, since it was not possible to relate small impact parameters with large electron energies for p^- projectiles. However, we think that the screening effect may be responsible for this behavior as a post-collisional effect: i.e., as fast electrons leave the collision region very rapidly, the final field felt by these electrons is the target nucleus field screened by the projectile field. Thus, fast electrons are able to acquire higher energies for p^- projectiles than for p^+ projectiles.

The correspondence between impact parameters and electron angles is more clear than for electron energies. Figure 13 shows that a very different behavior is obtained for protons or antiprotons: while large and small impact parameters are, respectively, related to small and large ejection angles for p^+ projectiles, the opposite conclusions are obtained for p^- projectiles. Olson and Gay[8] suggested that ejection at large angles might occur preferentially with negative projectiles due to the screening effect mentioned above. However, this new evidence indicates that this is not the most important reason for this behavior. In order to try to understand these reasons, we have analyzed the dynamical evolution of electrons with the same initial phase-space coordinates in the presence of different projectiles. We have checked that 42%, 9%, and 51% of the initial conditions that lead to ionization for p^- projectiles (at an impact energy of 100 keV), will lead to ionization, electron capture, and excitation for p^+ projectiles, respectively. Figure 14 shows the projection

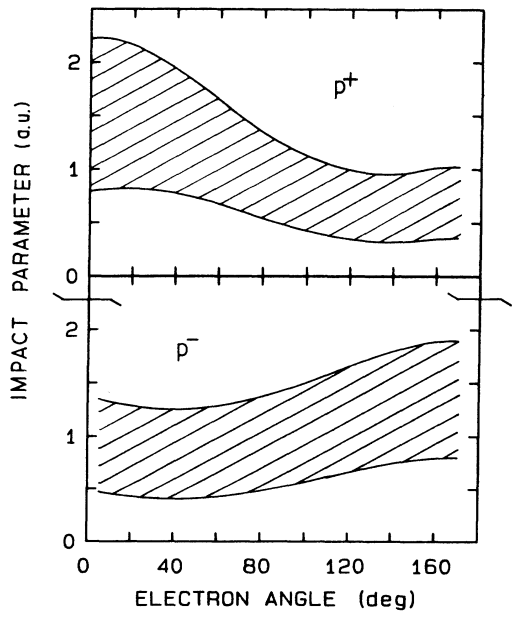

FIG 13. Regions determined by the mean impact parameter plus a standard deviation that lead to ionized electrons with a certain final angle in collisions of protons and antiprotons with He targets at an impact energy of 100 keV/amu.

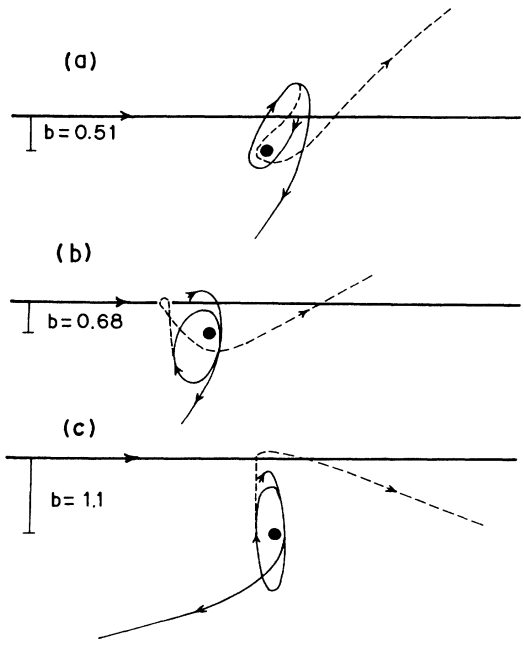

FIG. 14. Projection of the trajectories of the particles onto the collision plane for three different impact parameters b, as indicated. ——, trajectory of the projectile; ●, position of the target nucleus; — — —, trajectory of the electron for p^+ projectiles; ——, trajectory of the electron for p^- projectiles.

onto the collision plane of the evolution of three cases that lead to ionization for both projectiles. This figure illustrates how electrons with the same initial conditions are ejected at forward or backward angles for p^+ or p^- projectiles, respectively. These cases should not be considered to be the general behavior of the electrons (e.g., we have checked that large contributions to the electronic spectrum come from initial conditions in which the collision plane is perpendicular to the electron's orbit plane). Figure 14(a) illustrates the screening and antiscreening effects. On the other hand, Figs. 14(b) and 14(c) illustrate how initial conditions that lead to mechanisms that are very similar to a double or a single scattering of the electron for p^+ projectiles, lead to a very different behavior for p^- projectiles. While the electron is pulled away from its orbit in the case of protons, it is pushed toward the target nucleus and scattered by this centre to large angles in the case of antiprotons.

C. Comparison between the cross sections for the $p^+ + He$ and $He^{2+} + He$ systems

Figure 15 shows our ratios between the DDCS for the $p^+ + He$ and $He^{2+} + He$ systems at 100 keV/amu. The arrows in the electron energy axis indicate the position where the electron velocity is equal to the projectile velocity v_p. We have not plotted our ratios at ejection angles smaller than 5° since the statistical errors of these ratios are too large. We compare our results with the experimental ratios of Bernardi *et al.*[6] and Irby *et al.*[7] who estimated errors of 10% and 55% for their data, respectively. There is a good agreement between our calculations and the data of Bernardi *et al.*, except at 70°, where our ratios are up to 50% smaller than the experimental data. At 17° and small electron energies our results also agree with the data of Irby *et al.* However, these experimental ratios seem to be too small for electron energies greater than 30 eV.

As may be clearly seen in Fig. 15, there is a sharp increase of the ratios at small angles and at the position where the electron velocity equals the projectile velocity. This behavior is predicted by both the experimental data of Bernardi *et al.* and our CTMC calculations. This sudden rise was not observed by Irby *et al.* since their measurements were made at electron velocities smaller than v_p.

This enhancement indicates that the dependence of the DDCS on Z_p is very different on either side of the capture to the continuum (CTC) peak, and may be explained as follows. As it is well known, the CTC peak is very asymmetric. The asymmetry of the peak can be explained as a Coulombic deformation produced by the target residual nucleus on the electrons that are in the continuum of the projectile. As the projectile charge is increased, the relative importance of the target residual nucleus decreases and it is expected that the CTC peak will become more symmetric.

As may be seen in Fig. 16, both theoretical calculations

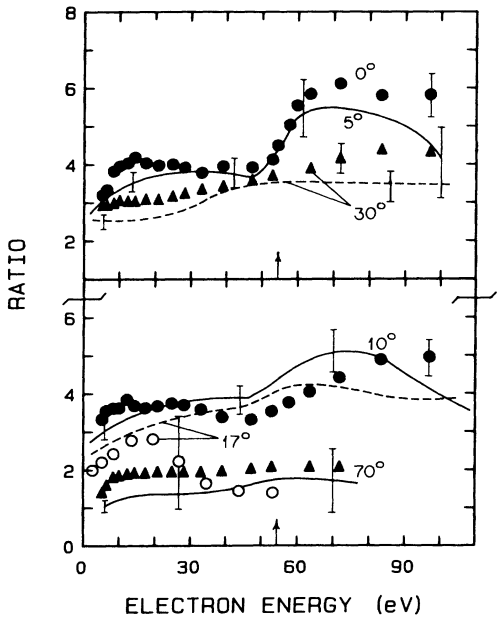

FIG. 15. Ratio between the DDCS for the $He^{2+} + He$ and $p^+ + He$ systems at an impact energy of 100 keV/amu as a function of the electron energy for fixed electron ejection angles (as indicated). The arrows in the electron energy axis indicate the position where the electron velocity equals the projectile velocity. ●, ▲, experimental data of Bernardi *et al.* (Ref. 6); ○, experimental data of Irby *et al.* (Ref. 7), — — —, ——, present CTMC calculations.

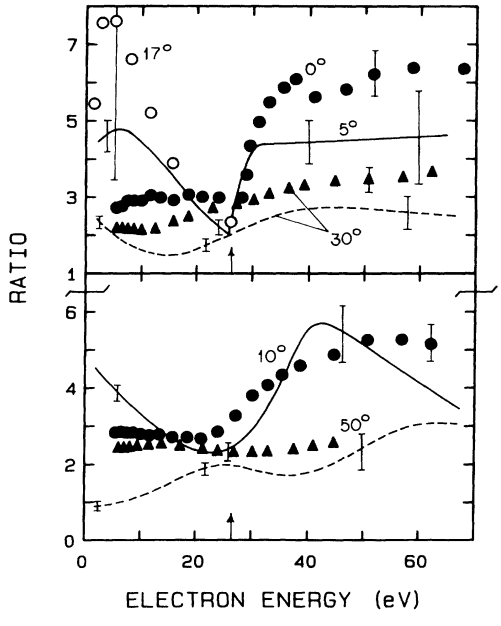

FIG. 16. Ratio between the DDCS for the $He^{2+} + He$ and $p^+ + He$ systems at an impact energy of 50 keV/amu as a function of the electron energy for fixed electron ejection angles (as indicated). The arrows in the electron energy axis indicate the position where the electron velocity equals the projectile velocity. ●, ▲, experimental data of Bernardi *et al.* (Ref. 6); ○, experimental data of Irby *et al.* (Ref. 7); · · · ·, ——, present CTMC calculations multiplied by a factor of 2.

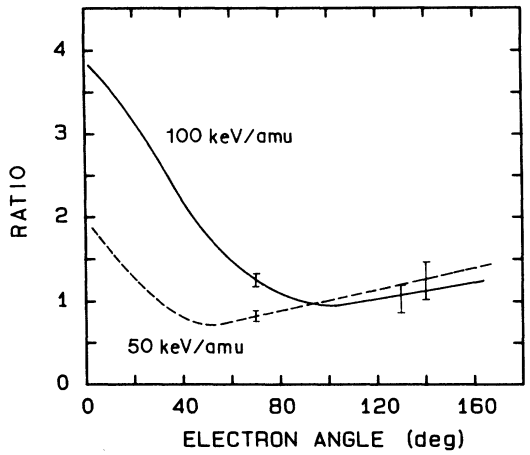

FIG. 17. CTMC calculations for the ratio between the SDCS for the $He^{2+}+He$ and $p^{+}+He$ systems as a function of the electron angle and at impact energies of 50 and 100 keV/amu, as indicated.

and experimental data also predict a sudden increase of the ratios around the CTC peak at 50 keV/amu. However, our results disagree in both shape and magnitude with the data of Bernardi *et al.* (note that CTMC ratios have been multiplied by a factor of 2 in order to directly compare to experiment). We have not included correlation effects in our CTMC model and the impact energy of 50 keV/amu is the limit of the validity range of our calculations. However, we cannot explain the difference in the magnitude of the ratios due to the following facts. First, the ratio between our calculated electron-emission total cross sections for the He^{2+} and $p^{+}+He$ systems is equal to 1.23, which is very similar to the mean experimental ratio 1.36 that can be obtained from the works of Shah and Gilbody,[27] Rudd *et al.*,[19–22] and Gibson and Reid.[23] Second, we have checked by means of the CTMC method that 85% of the total cross section at 50 keV/amu arises from electrons that are ejected at angles smaller than 50°. As the experimental ratios of Bernardi *et al.* are always greater than 2, it can be expected that their ratio between total cross sections will be also greater than 2. This would be very different from the mean experimental ratio 1.36 mentioned above. This conclusion contrasts with the fact that the ratios of Bernardi *et al.* should be independent from any normalization, since they were obtained under the same experimental conditions. Concerning the shape of the ratios, Fig. 16 shows that, while the ratios of Bernardi *et al.* do not significantly change at small angles and small electron energies, the CTMC ratios decrease as the electron energy increases. Due to this discrepancy, we have also plotted in Fig. 16 the experimental ratios of Irby *et al.*[7] at 17° and an impact energy of 60 keV/amu. These ratios are still greater in magnitude than the ratios of Bernardi *et al.*, but exhibit a negative slope at small electron energies in agreement with our theoretical calculations.

Figures 15 and 16 also show that both experimental data and CTMC calculations predict large departures from first-order theories such as the first Born or the classical binary encounter approximations for direct ionization. According to these theories, the ratio between the DDCS should be equal to four over all the electronic spectrum. However, it may be clearly seen that the ratios depend on both the energy and the angle of the ejected electrons. We also note that the behavior of the ratios around the CTC peak is very different from the Z_p^3 scaling (i.e., a ratio of eight) predicted by first-order theories for capture to the continuum of the projectile. These departures may be seen more clearly in Fig. 17, in which we have plotted the ratios between the SDCS for the $p^{+}+He$ and $He^{2+}+He$ systems. This figure shows that our ratios are smaller than 4 over all the angular spectra. However, Reinhold *et al.*[2] have shown that an enhancement appears in the CTMC ratios at forward angles as the collision energy is increased. We also note that CTMC predicts a small rise of the ratios at large ejection angles. This rise is present (within statistical errors) only at 50 keV/amu. It has not been observed experimentally by Bernardi *et al.*[6] since their measurements were made at ejection angles smaller than 50°. Further experimental data would be necessary to confirm this behavior.

ACKNOWLEDGMENTS

This work was supported by the office of Fusion Energy of the U.S. Department of Energy. We would like to thank Dr. J. E. Miraglia for providing us the code to calculate the Born approximation.

[1]R. E. Olson, T. J. Gay, H. G. Berry, E. B. Hale, and V. D. Irby, Phys. Rev. Lett. **59**, (1987) p. 36.
[2]C. O. Reinhold, C. A. Falcon, and J. E. Miraglia, J. Phys. B **20**, 3737 (1987).
[3]N. Stolterfoht, D. Schneider, J. Tanis, H. Altervogt, A. Salin, P. D. Fainstein, R. Rivarola, J. P. Grandin, J. N. Scheurer, S. Andriamonje, D. Bertault, and J. F. Chemin, Europhys. Lett. **4**, 899 (1987).
[4]P. D. Fainstein, V. H. Ponce, and R. D. Rivarola, J. Phys. B **21**, 287 (1988).
[5]C. O. Reinhold and R. E. Olson, J. Phys. B **22**, L39 (1989).
[6]G. C. Bernardi, S. Suarez, C. R. Garibotti, and W. Meckbach (unpublished).
[7]V. D. Irby, T. J. Gay, J. Wm. Edwards, E. B. Hale, M. L. McKenzie, and R. E. Olson, Phys. Rev. A **37**, 3612 (1988).
[8]R. E. Olson and T. J. Gay, Phys. Rev. Lett. **61**, 302 (1988).
[9]R. E. Olson, Phys. Rev. A **36**, 1519 (1987).
[10]P. D. Fainstein, V. H. Ponce, and R. D. Rivarola, J. Phys. B **21**, 2989 (1988).
[11]R. Abrines and I. C. Percival, Proc. Phys. Soc. **88**, 861 (1966).
[12]R. E. Olson and A. Salop, Phys. Rev. A **16**, 531 (1977).
[13]R. E. Olson, Phys. Rev. A **16**, 1871 (1983).
[14]R. E. Olson, Phys. Rev. A **33**, 4397 (1986).
[15]T. F. M. Bonsen and D. Banks, J. Phys. B **4**, 706 (1971).
[16]G. Schiwietz and W. Fritsch, J. Phys. B **20**, 5463 (1987).
[17]D. R. Schultz and R. E. Olson, Phys. Rev. A **38**, 1866 (1988).
[18]C. O. Reinhold and C. A. Falcon, Phys. Rev. A **33**, 3859 (1986).

[19]M. E. Rudd and D. H. Madison, Phys. Rev. A **14**, 128 (1976).
[20]M. E. Rudd and T. Jorgensen, Phys. Rev. **131**, 666 (1963).
[21]M. E. Rudd, C. A. Sauter, and C. L. Bailey, Phys. Rev. **151**, 20 (1966).
[22]M. E. Rudd, L. H. Toburen, and N. Stolterfoht, At. Data Nucl. Data Tables **18**, 413 (1976).
[23]D. K. Gibson and I. D. Reid, J. Phys. B **19**, 3265 (1986); also see the 1985 Australian Atomic Energy Commission Report No. AAEC E608 (unpublished).
[24]G. B. Crooks and M. E. Rudd, Phys. Rev. Lett. **25**, 1599 (1970).
[25]V. Montemayor and G. Schiwietz (unpublished).
[26]J. H. McGuire and L. Weaver, Phys. Rev. A **16**, 41 (1977).
[27]M. B. Shah and H. B. Gilbody, J. Phys. B **18**, 899 (1985).
[28]S. Yu. Ovchinnikov and D. B. Khrebtukov, *Abstracts of Contributed Papers of the 15th International Conference on the Physics of Electronic and Atomic Collisions, Brighton, United Kingdom, 1987* edited by H. B. Gilbody *et al.* (North-Holland, Amsterdam, 1987), p. 596.
[29]P. Dahl, J. Phys. B **18**, 1181 (1985).
[30]T.F.M. Bonsen and L. Vriens, Physica **47**, 307 (1970).
[31]C. R. Garibotti and J. E. Miraglia, Phys. Rev. A **21**, 572 (1980).
[32]G. Mehler, B. Muller, W. Greiner, and G. Soff, Phys. Rev. A **36**, 1454 (1987).